ADVANCED HEALTHCARE MATERIALS
www.advhealthmat.de

Detection of Avian Influenza Virus from Cloacal Swabs Using a Disposable Well Gate FET Sensor

*Sungwook Park, Jaebin Choi, Minhong Jeun, Yongdeok Kim, Seong-Su Yuk, Sang Kyung Kim, Chang-Seon Song, Seok Lee, and Kwan Hyi Lee**

Current methods to detect avian influenza viruses (AIV) are time consuming and lo inw sensitivity, necessitating a faster and more sensitive sensor for on-site epidemic detection in poultry farms and urban population centers. This study reports a field effect transistor (FET) based AIV sensor that detects nucleoproteins (NP) within 30 minutes, down to an LOD of 10^3 EID_{50} mL^{-1} from a live animal cloacal swab. Previously reported FET sensors for AIV detection have not targeted NPs, an internal protein shared across multiple strains, due to the difficulty of field-effect sensing in a highly ionic lysis buffer. The AIV sensor overcomes the sensitivity limit with an FET-based platform enhanced with a disposable well gate (DWG) that is readily replaceable after each measurement. In a single procedure, the virus-containing sample is immersed in a lysis buffer mixture to expose NPs to the DWG surface. In comparison with commercial AIV rapid kits, the AIV sensor is proved to be highly sensitive, fast, and compact, proving its potential effectiveness as a portable biosensor.

Avian influenza viruses (AIV), normally transferred between birds, intermittently create fatal outbreaks in the human population. Mutations cause surface glycoproteins such as hemagglutinin (HA) and neuraminidase (NA) to vary widely across subtypes, making it difficult for sensors and assays to capture the constantly changing virus.[1–4] Nucleoproteins (NP), on the other hand, are proteins internal to the virus and less subject to mutation. In this work, we present an AIV sensor that targets NPs, which are nearly identical across a wide range of subtypes and hence ideal for a multistrain point-of-care AIV detection device.[5,6]

A common influenza detection protocol consists of on-site diagnosis with a rapid kit followed by definite diagnosis by real-time polymerase chain reaction (RT-PCR). Rapid kits are portable and fast but are limited in sensitivity (10^4–10^6 EID_{50} mL^{-1}). RT-PCR is to date the most reliable detection method for recognizing viral RNA fragments, but requires several hours of amplification in a lab setting, making it unsuited for on-site detection.[1,7] Such challenges have encouraged the development of alternate methods of rapid AIV diagnosis—with recent advancements made in electric biosensors, such as high sensitivity, label-free electrical detection by field effect transistors (FETs).[8–10]

FET biosensors offer two advantages over other detection methods: real-time detection and a scalable manufacturing process.[11–15] Comparing them to optical or fluorescence sensors, FET sensors are small, cheap, and unhindered by the visual opacity of biological solutions. Compared to electrochemical sensors that collect individual electrons, the exponential conversion between voltage and induced current acts as a built-in amplification scheme. Despite such strengths, FETs have not been successful in the detection of clinical samples because the abundance of ions in such samples hinders electrostatic charge detection, also known as the Debye screening effect. As a result, an FET experiences an exponential decrease in its sensitivity with increasing ionic content.[15–19] The same applies to virus detection, because the high ionic content of virus lysis buffers hinders FET analysis. An FET also faces the risk of contamination after exposure to an on-site sample, requiring either a reliable washing procedure or disposure of the device. Thus, FET sensors have been considered inappropriate for point-of-care (POC) AIV diagnostics.

In this work, we focus our efforts on overcoming the drawbacks of FET biosensors with a disposable well gate (DWG). The DWG enables the reusage of an FET device while maintaining

S. Park, Dr. M. Jeun, Y. Kim, Dr. K. H. Lee
Center for Biomaterials
Biomedical Research Institute
Korea Institute of Science and Technology (KIST)
5 Hwarang-ro 14-gil, Seongbuk-gu, Seoul 02792, Republic of Korea
E-mail: kwanhyi@kist.re.kr
S. Park, Dr. K. H. Lee
Department of Biomedical Engineering
Korea University of Science and Technology (UST)
217 Gajeong-ro, Yuseong-gu, Daejeon 34113, Republic of Korea
J. B. Choi, Dr. S. Lee
Sensor System Research Center
Korea Institute of Science and Technology (KIST)
5 Hwarang-ro 14-gil, Seongbuk-gu, Seoul 02792, Republic of Korea
Dr. S. K. Kim
Center for BioMicrosystems
Korea Institute of Science and Technology (KIST)
5 Hwarang-ro 14-gil, Seongbuk-gu, Seoul 02792, Republic of Korea
S.-S. Yuk, Dr. C.-S. Song
Avian diseases laboratory
Colleage of Veterinary Medicine
Konkuk University
120 Neungdong-ro, Gwangjin-gu, Seoul 05029, Republic of Korea
The ORCID identification number(s) for the author(s) of this article can be found under https://doi.org/10.1002/adhm.201700371.

DOI: 10.1002/adhm.201700371

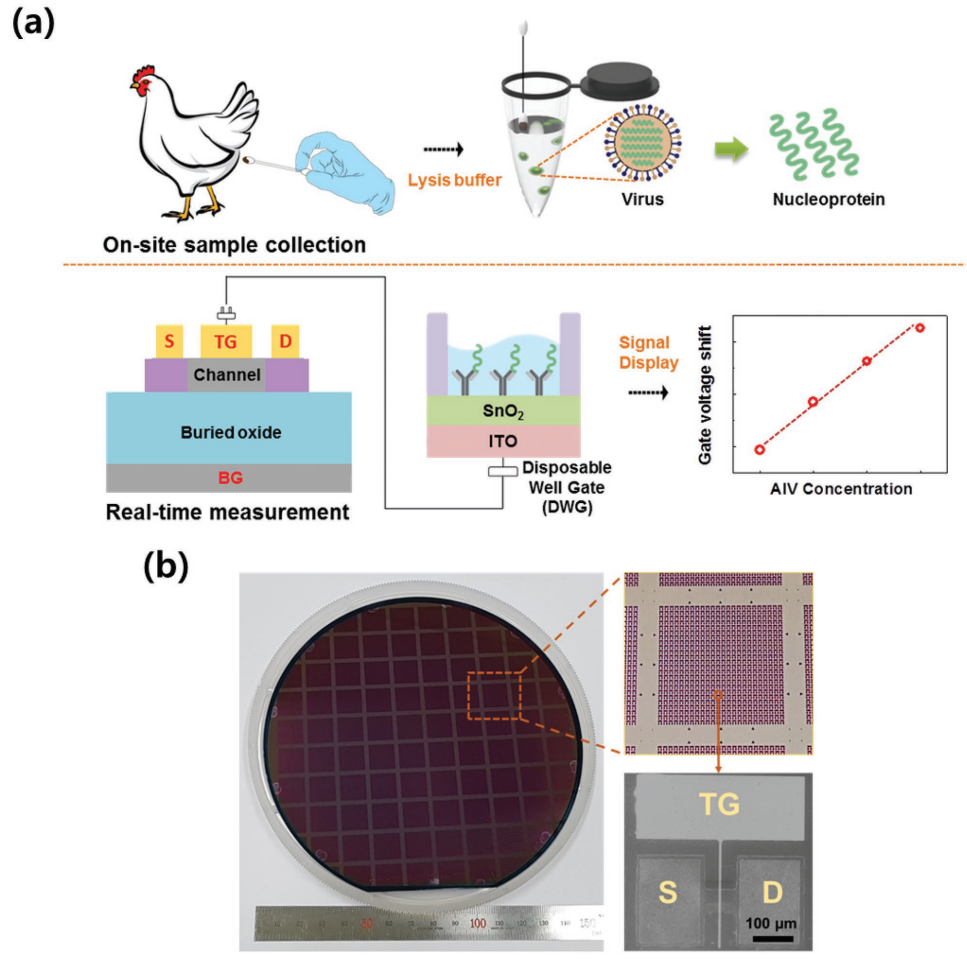

Figure 1. a) Illustration of the AIV sensor operation procedure: a cloacal swab from a live host is immersed in a 1:1 mix of lysis buffer and MEM buffer for 10 minutes and dropped onto the DWG for a measurement of AIV concentration. b) Image of AIV sensors produced on a wafer-scale process with ≈25 000 devices per wafer.

high sensitivity towards AIV NPs. It is designed to maintain its voltage in a standard lysis buffer solution, allowing a cloacal swab to be immersed directly in a lysis buffer in a one-step lysis procedure (**Figure 1**a). It separates the transducer from the sample, protecting it from contamination and degradation, and being disposed after a single read-out in place of the significantly more costly FET device.

The AIV sensor adopts a structurally engineered dual gate to overcome the short Debye length in a lysis buffer with high ionic content.[20,21] The dual-gate transducer's superb sensitivity and selectivity allow detection directly from a lysis buffer, eliminating the need for labeling or dilution of the buffer solution. The AIV sensor successfully detects the H9N2 subtype of the Influenza A virus family by detecting their NPs down to a sensitivity of $\approx 10^3$ EID_{50} mL^{-1}, outperforming rapid kits by at least one order of magnitude in sensitivity. We also demonstrate the sensor's on-site adequacy by testing it on a cloacal swab acquired from a live chicken, replicating a common on-site protocol.

To the best of our knowledge, this is the first report of on-site AI virus detection by an FET biosensor. Figure 1a shows a schematic of the data acquisition procedure. A cloacal swab from a live host is immersed in a lysis buffer for 10 minutes, the time it takes for viruses to release NPs, and then transferred to the DWG for electrical measurement. It is notable that this procedure does not require filtering or purification. The DWG surface contains antibodies ready to capture NPs from the solution. The total virus confirmation time of 20 minutes is several hours faster than that of RT-PCR. Compared to commercially available rapid kits, purchased from Bionote Inc., South Korea, the AIV sensor achieves a greater sensitivity while experiencing comparable confirmation time. Figure 1b shows the AIV sensor fabricated on a wafer scale, indicating the device's potential to be manufactured on an even larger scale, offering benefits of cost reduction and statistical data on device variability.

Figure 2a shows the AIV sensor's I_{DS}–V_{GS} curves shifting with time as lysed H9N2 virus nucleoproteins bond with antibodies on the DWG floor. NPs accumulate as static charge on the DWG, altering the channel resistance of the transistor by field effect. This results in a leftward shift of the I_{DS}–V_{GS} curve, with its magnitude, ΔV_R, being an indicator of the concentration of NPs inside the solution. The antibody-NP reaction induces sufficient shift and confirms virus detection within only 20 minutes, making the sensor apt for POC diagnosis.

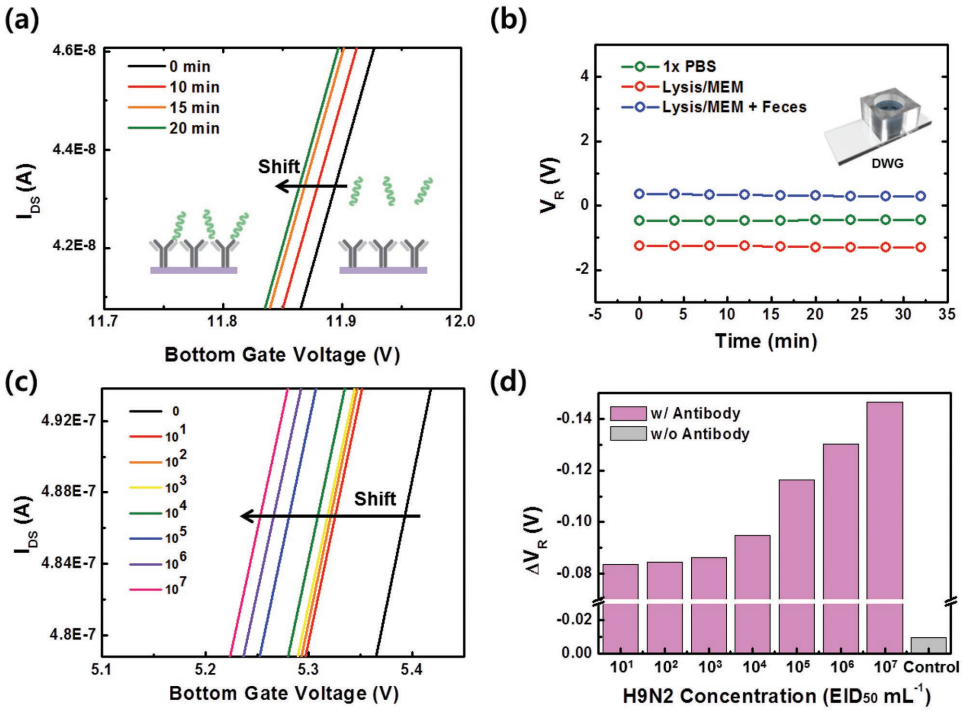

Figure 2. a) I_{DS}–V_{GS} response of the AIV sensor stabilizing its voltage shift in 20 minutes. b) Stability test of the sensor in various solution backgrounds. c) Response of the AIV sensor against exponentially increasing concentrations of the H9N2 virus extracted from allantoic fluid. d) ΔV_R values acquired from previous data, compared against an antibody-absent control DWG.

The AIV sensor's one-buffer (1:1 lysis buffer:minimum essential medium(MEM) buffer mixture) procedure is another attribute that strongly advocates POC diagnosis. The difficulty of wet-lab procedures has prevented labeling methods from being applied on site. The AIV sensor performs both pretreatment (lysis) and measurement in a single buffer, significantly reducing the workload prior to measurement. Previously reported FETs were not able to perform measurements immediately from feces due to the sample's heterogeneity and an FET's limited sensitivity in high ion concentration buffers. In this system, the DWG helps secure data by separating the transducer from the incubator/measurement chamber, and the limited sensitivity has been supplemented by the amplification scheme provided by the dual-gate FET.

As a test of the AIV sensor's stability over a long period of time, we acquire V_R values for three different buffers, 1× phosphate buffered saline (PBS), 1:1 lysis buffer, and MEM buffer mixture, and the latter with uninfected chicken feces, for 32 minutes (Figure 2b). The sensor's saturation to a stable value suggests its stability against time. Figure 2c displays the ΔV_R shift for H9N2 concentrations starting from 10^1 EID_{50} mL^{-1} to 10^7 EID_{50} mL^{-1}, where Figure 2d shows the same data in the form of a bar graph, along with a value acquired from a DWG without antibody immobilization (control). The magnitude of negative voltage shift increases with respect to increasing virus concentrations, indicating that an approximate virus concentration may be extrapolated from a given value of ΔV_R. ΔV_R at the detection limit of 10^3 EID_{50} mL^{-1} is well above the ΔV_R of control devices, thus confirming that the sensor properly rules out nonspecific binding.

Figures 3a,b show the AIV sensor's response compared with that of the rapid kit which uses identical antibodies. The rapid kit shows a severely faint signal at a virus concentration of 10^4 EID_{50} mL^{-1}, but a visible signal above 10^5 EID_{50} mL^{-1}. On the contrary, the AIV sensor is able to detect NPs down to 10^3 EID_{50} mL^{-1} (Figure 3a). The linearity of numerical outputs of the AIV sensor can further be calibrated to yield quantitative measurements.

Finally, we test the efficacy of the AIV sensor as an on-site-applicable system using cloacal swabs acquired from H9N2-infected chickens. The swabs, acquired from 3 week-old chickens 4 days after infection, are tested on the AIV sensor (Figure 3c) and rapid kit (Figure 3d), respectively. A total of five cloacal swab samples, each acquired from different hosts, are immersed in the 1:1 mix solution for 10 minutes and immediately transferred to a set of DWGs. CS1, a sample that experiences a voltage shift equivalent to $10^{5.25}$ EID_{50} mL^{-1} (calculated from the standard curve in Figure 1d) on the AIV sensor, shows only a faint signal line on the rapid kit. CS2 and CS3 yields low read-outs for the AIV sensor are also undetected by the rapid kit. CS4, interestingly, produces an approximate value of $10^{5.66}$ EID_{50} mL^{-1} on the AIV sensor while being undetected by the rapid kit. This suggests the AIV sensor's ability to detect at a higher sensitivity than the rapid kit. CS5 produces no meaningful voltage shift on a DWG without antibodies immobilized to its surface, thus confirming the AIV sensor's specificity. We therefore confirm the AIV sensor's detection of NPs at lower levels than the rapid kit limit of detection (LOD) of 10^4 EID_{50} mL^{-1}, from the cloacal swabs of live chicken hosts.

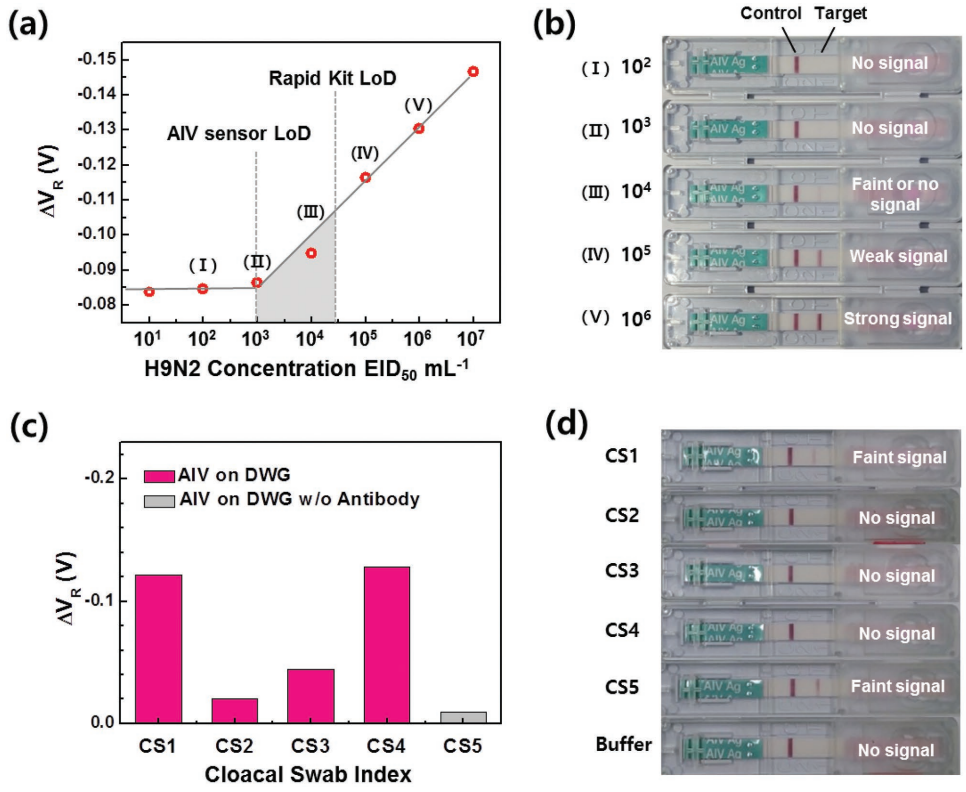

Figure 3. Comparison of a) AIV sensor and b) rapid kit in detecting identical samples of increasing H9N2 concentration. Virus was extracted from allantoic fluid. Comparison of c) AIV sensor and d) rapid kit detection results on cloacal swabs acquired from live infected hosts.

Table 1 offers a comparison of the AIV sensor with state-of-the-art FET virus sensors. This work is the first among FET sensors to detect AIV nucleoproteins directly from an on-site, live-animal sample. LOD is improved by at least one order of magnitude compared to the rapid kit. A measurement performed on a structurally similar FET sensor but without the DWG optimized to a lysis buffer solution shows an LOD of 1.5 fM for hepatitis b surface antigen,[20] suggesting a comparable level of sensitivity for the AIV sensor against nucleoproteins.

In conclusion, an FET-based AIV sensor is joined with an electro-chemically optimized DWG to detect virus NPs of the H9N2 strain in high sensitivity. The 30 min swab-to-definitive diagnosis time, one-buffer procedure, and disposability of the DWG are vital elements for rapid on-site diagnosis of viral infections. The system yields a detection limit of 10^3 EID_{50} mL^{-1}, which is more than one order of magnitude lower than that of a commercial rapid kit. The sensor retains its superb sensitivity when tested against a real cloacal swab sample from of a live infected chicken, thereby proving its effectiveness as a POC diagnosis device.

Table 1. An overview of existing FET-based AIV sensors.

Target	Solution	LOD	On-site sample	References
DNA	10×10^{-3} M PBS	Few fM	X	[8]
DNA	0.1× PBS	1 fM	X	[22]
DNA	0.1×10^{-3} M PBS	100×10^{-12} M	X	[23]
HA[a] protein	0.01× PBS	Few aM	X	[24]
Silica-binding protein	1× PBS	966.6×10^{-12} M	X	[25]
Hepatitis B virus protein	1× PBS	1.5 fM	X	[20]
Nucleoprotein	C.S.[b] in Lysis buffer	10^3 EID_{50} mL^{-1}	○	This work

[a]Hemagglutinin; [b]Cloacal swab.

Experimental Section

Materials: Dimethylformamide, succinic anhydride, (3-Aminopropyl)-triethoxysilane (APTES), and ethanolamine were purchased from Sigma-Aldrich. 1-Ethyl-3-3-dimethylaminopropyl-carbodiimide (EDC) and *N*-hydroxysulfosuccinimide (Sulfo-NHS) were purchased from Thermo Scientific. Optical rapid test kit (RG15-01) including antibodies and lysis buffer was purchased from Bionote, Inc (Korea). The lysis buffer had a composition of 50×10^{-3} M Tris(hydroxymethyl)-aminomethane (TRIS) and 0.05% sodium azide.

Fabrication of Dual-Gate FET: The transistor was fabricated on a 6 in. p-type (100) silicon-on-insulator wafer with a 750 nm buried oxide layer as a bottom gate. The thickness of the top silicon layer was 100 nm.

To form the active region, photolithography and inductively coupled plasma reactive-ion etching were undertaken. A 10 nm thick SiO_2 top gate oxide layer was grown by dry oxidation processes. Subsequently, a Ti/TiN/Al/TiN multlayer was deposited on the top layer by a sputtering system,

and then it was etched by photolithography and etching processes to form the gate region. Arsenic ions (concentration: 3×10^{15}) were implanted to from the source and drain regions. To form the contact electrodes, a Ti/TiN/Al/TiN multilayer was built by sputtering and lift-off processes. Finally, at 450 °C for 30 minutes in a 2% H_2/N_2 atmosphere, forming gas annealing was carried out to reduce dangling bonds and defects.

In order to fabricate the DWG, an 80 nm thick tin dioxide (SnO_2) sensing membrane was deposited on an ITO substrate using a radio frequency (RF) magnetron sputter with 50 W of power, in 18 mTorr and 20 sccm of Argon gas flow. A polydimethylsiloxane well was attached to the SnO_2 sensing membrane after exposure to 30 W O_2 plasma for 5 minutes. The surface of the sensing area was 0.5 cm^2 in area (0.8 cm in diameter).

FET Fabrication Yield: A device yield of 70% was achieved from the wafer scale fabrication process as found from probe-measuring more than 300 devices. In particular, pH sensitivity was tested for nine selected devices, yielding an average sensitivity of 781 mV pH^{-1} and a standard deviation of 82 mV pH^{-1}. Device variation was expected to be minimized with better control of the oxide quality. The device with the highest sensitivity (910 mV pH^{-1}) stayed reliable throughout the production of the entire set of data shown in this work.

Antibody Conjugation on the DWG Floor: The surface of SnO_2 was treated with O_2 plasma under the same conditions with the previous process to provide —OH groups on the surface. Next was added 5% APTES (APTES 500 µL + ethanol 9.5 mL^{-1}) to the surface of SnO_2, at room temperature, for 1 hour, to form $-NH_2$ groups and was baked on a hot plate at 120 °C for 30 minutes. Next, 1 M succinic acid was added and incubated at 37 °C for 16 h. 4 M EDC and 1 M sulfo-NHS were added for 15 minutes at room temperature in order to form —COOH groups on the surface.[26] 100×10^{-9} M AIV antibodies in PBS were added at room temperature for 1 hour to build peptide bonds.[27,28] 1 M ethanolamine was used to block remnant —COOH ends. Additionally, 100 mg mL^{-1} bovine serum albumin was used to block nonspecific binding sites.[29] Finally, nucleoproteins dispersed in a lysis buffer were added to the sensor surface for 20 minutes at room temperature to induce antigen–antibody reactions.

AIV Sensor Measurement Setup: A commercial Ag/AgCl reference electrode and Hewlett-Packard 4156B high precision semiconductor parameter analyzer were utilized for FET measurements inside a dark box. The drain-source current (I_D) was measured against a sweep in the bottom gate voltage (V_G), while the reference electrode in the solution was grounded. The top gate was electrically connected to the electrode on the DWG.

A target buffer was produced by putting Influenza A viruses (H5N1, H5N8) and swab samples (from a H9N2-infected host) into 1X PBS, and then adding a lysis buffer and leaving for 10 minutes at room temperature. The DWG's extended gate that was anti-nucleoprotein antibody-immobilized was exposed to 100 µL of virus solution. Current versus voltage (I_D–V_G) measurements were taken 20 minutes later. Measurements were repeated for nucleoprotein virus solutions in the range 10^2–10^5 EID_{50} mL^{-1}. The same was repeated for the swab sample.

Results were compared with a commercially available antibody-based optical rapid kit produced by Bionote, Inc (Korea). The rapid kit results were obtained by inverting the virus with a lysis buffer for 10 minutes. A droplet of 120 µL volume was dropped onto the test area. A visible line appears 2–20 minutes later, should the droplet include sufficient NPs. The rapid kit produces two lines, one reacting to the lysis buffer, and another reacting to virus NPs.

Acknowledgements

S.P., J.B.C., and M.J. contributed equally to this work. This research was supported by KIST (ORP #2E26631, TRC #2V05420) and the R&D Convergence Program of National Research Council of Science & Technology (NST) of Republic of Korea (CAP-16-02-KIST). The authors appreciate Dr. Hoon-jung Oh at the Bio-IT Micro Fabrication Center of Yonsei University for her consultation on FET design and Ms. Yu-kyeong Park at the Inter-university Semiconductor Research Center, Seoul National University for her advice on FET fabrication processes.

Conflict of Interest

The authors declare no conflict of interest.

Keywords

avian influenza, cloacal swab, disposable well gate, FET sensors, on-site detection

Received: March 21, 2017
Revised: April 14, 2017
Published online: May 16, 2017

[1] M. D. de Jong, T. T. Hien, *J. Clin. Virol.* **2006**, *35*, 2.
[2] I. Sitaras, D. Kalthoff, M. Beer, B. Peeters, M. C. M. de Jong, *Plos One* **2014**, *9*, e84628.
[3] N. Skeik, F. I. Jabr, *Int. J. Infect. Dis.* **2008**, *12*, 233.
[4] R. G. Webster, W. J. Bean, O. T. Gorman, T. M. Chambers, Y. Kawaoka, *Microbiol. Rev.* **1992**, *56*, 152.
[5] V. R. Harley, P. J. Hudson, B. E. Coupar, P. W. Selleck, H. Westbury, D. B. Boyle, *Arch. Virol.* **1990**, *113*, 133.
[6] T. Miyoshi-Akiyama, T. Yamashiro, Q. Mai le, K. Narahara, A. Miyamoto, S. Shinagawa, S. Mori, H. Kitajima, T. Kirikae, *Influenza Other Respir. Viruses* **2012**, *6*, 434.
[7] M. J. Espy, J. R. Uhl, L. M. Sloan, S. P. Buckwalter, M. F. Jones, E. A. Vetter, J. D. Yao, N. L. Wengenack, J. E. Rosenblatt, F. R. Cockerill 3rd, T. F. Smith, *Clin. Microbiol. Rev.* **2006**, *19*, 165.
[8] C. H. Lin, C. H. Hung, C. Y. Hsiao, H. C. Lin, F. H. Ko, Y. S. Yang, *Biosens. Bioelectron.* **2009**, *24*, 3019.
[9] J. H. Ahn, S. J. Choi, J. W. Han, T. J. Park, S. Y. Lee, Y. K. Choi, *Nano Lett.* **2010**, *10*, 2934.
[10] D. Karnaushenko, B. Ibarlucea, S. Lee, G. Lin, L. Baraban, S. Pregl, M. Melzer, D. Makarov, W. M. Weber, T. Mikolajick, O. G. Schmidt, G. Cuniberti, *Adv. Healthcare Mater.* **2015**, *4*, 1517.
[11] H. J. Jang, J. Ahn, M. G. Kim, Y. B. Shin, M. Jeun, W. J. Cho, K. H. Lee, *Biosens. Bioelectron.* **2015**, *64*, 318.
[12] P. A. Hu, J. Zhang, L. Li, Z. L. Wang, W. O'Neill, P. Estrela, *Sensors* **2010**, *10*, 5133.
[13] D. J. Kim, H. C. Park, I. Y. Sohn, J. H. Jung, O. J. Yoon, J. S. Park, M. Y. Yoon, N. E. Lee, *Small* **2013**, *9*, 3352.
[14] M. J. Schoning, A. Poghossian, *Analyst* **2002**, *127*, 1137.
[15] M. S. Makowski, A. Ivanisevic, *Small* **2011**, *7*, 1863.
[16] M. L. Sin, K. E. Mach, P. K. Wong, J. C. Liao, *Expert Rev. Mol. Diagn.* **2014**, *14*, 225.
[17] A. Matsumoto, Y. Miyahara, *Nanoscale* **2013**, *5*, 10702.
[18] R. Elnathan, M. Kwiat, A. Pevzner, Y. Engel, L. Burstein, A. Khatchtourints, A. Lichtenstein, R. Kantaev, F. Patolsky, *Nano Lett.* **2012**, *12*, 5245.
[19] E. Stern, A. Vacic, N. K. Rajan, J. M. Criscione, J. Park, B. R. Ilic, D. J. Mooney, M. A. Reed, T. M. Fahmy, *Nat. Nanotechnol.* **2010**, *5*, 138.
[20] I. K. Lee, M. Jeun, H. J. Jang, W. J. Cho, K. H. Lee, *Nanoscale* **2015**, *7*, 16789.
[21] O. Knopfmacher, A. Tarasov, W. Y. Fu, M. Wipf, B. Niesen, M. Calame, C. Schonenberger, *Nano Lett.* **2010**, *10*, 2268.

[22] A. Gao, N. Lu, P. Dai, T. Li, H. Pei, X. Gao, Y. Gong, Y. Wang, C. Fan, *Nano Lett.* **2011**, *11*, 3974.
[23] K. H. Lee, J. O. Lee, S. Choi, J. B. Yoon, G. H. Cho, *Biosens. Bioelectron.* **2012**, *31*, 343.
[24] S. Hideshima, H. Hinou, D. Ebihara, R. Sato, S. Kuroiwa, T. Nakanishi, S. I. Nishimura, T. Osaka, *Anal. Chem.* **2013**, *85*, 5641.
[25] J. Y. Kim, J. H. Ahn, D. I. Moon, T. J. Park, S. Y. Lee, Y. K. Choi, *Biosens. Bioelectron.* **2014**, *55*, 162.
[26] C. Kim, J. F. Galloway, K. H. Lee, P. C. Searson, *Bioconjugate Chem.* **2014**, *25*, 1893.
[27] J. F. Galloway, A. Winter, K. H. Lee, J. H. Park, C. M. Dvoracek, P. Devreotes, P. C. Searson, *Nanomed.: Nanotechnol. Biol. Med.* **2012**, *8*, 1190.
[28] M. P. Hwang, J. W. Lee, K. E. Lee, K. H. Lee, *ACS Nano* **2013**, *7*, 8167.
[29] G. H. Jang, M. P. Hwang, S. Y. Kim, H. S. Jang, K. H. Lee, *Biomaterials* **2014**, *35*, 440.